METEOROLOGICAL APPLICATIONS
Meteorol. Appl. **16**: 215–225 (2009)
Published online 31 October 2008 in Wiley InterScience
(www.interscience.wiley.com) DOI: 10.1002/met.110

RMetS
Royal Meteorological Society

On the formation and persistence of superfog in woodland smoke†

Gary L. Achtemeier*
USDA Forest Service, Southern Research Station, Center for Forest Disturbance Science, Athens, GA 30602, USA

ABSTRACT: Dense fogs, comparable to historical fogs in England, have been implicated in numerous roadway accidents in the southern United States. Many of the fogs have occurred in association with prescribed burning. Direct measurements of superfog (fog reducing visibility to less than 3 m) were taken during burning of forest litter on 22 March 2003. Visibility was measured at 0.1 m implying an extinction coefficient of 39 120 km^{-1}. The number of condensation nuclei required for fog to produce the observed visibility was about 1% of the number of particles released in wood smoke as reported in the literature. A recursive non-gradient mixing model shows (1) maximum excess liquid water (LWC) released was approximately 7.0 g kg^{-1}, 23 times the LWC in natural fog, (2) superfog can form at the site of combustion then continue to form as it drifts downwind, and (3) superfog can modify air mass stability near the ground and persist for hours until dispersed by changing wind conditions or by solar heating after sunrise. Published in 2008 by John Wiley & Sons Ltd.

KEY WORDS highway accidents; visibility; dense fog; smoke; prescribed fire

Received 22 January 2008; Revised 6 August 2008; Accepted 15 September 2008

1. Introduction

Dense smogs reducing visibility to a few metres or less have been documented for hundreds of years in England (Urbinato, 1994). Many of these smogs were linked to the use of sea-coal – a copious smoke producer when burned – to heat homes in crowded urban areas. Among the most notorious of London smogs was the Great Smog of 5–9 December 1952. According to the UK Meteorological Office, the visibility in central London remained below 500 m continuously for 114 h and below 50 m continuously for 48 h from the morning of 6 December. At Heathrow Airport the visibility remained below 10 m for almost 48 h. The death toll was estimated at approximately 4000 (Urbinato, 1994). Bell and Davis (2001) suggest that about 12 000 excess deaths linked to the fog occurred between December 1952 and February 1953.

Kunkel (1984) and Kokkola *et al.* (2003) have shown that heavily polluted conditions can favour the formation of dense radiation fogs consisting of large numbers of relatively small droplets. Pollutants act in two ways to decrease visibility: (1) increasing the number of particles which increases the extinction coefficient for a given liquid water content (LWC), and, (2) decreasing droplet size which decreases mean terminal velocity thus minimizing the fallout of liquid water. These fogs can initiate when relative humidities are slightly less than 100%.

In sections of the USA and parts of Canada (Pagowski *et al.*, 2004), dense fogs reducing visibility to a few metres have been implicated as a causal factor of multiple vehicle accidents. An additional factor contributing to the frequency of extreme fog events is the combination of fog with smoke from prescribed burning (Achtemeier *et al.*, 1998). Holle (1970) and Eagan *et al.* (1973) estimated that approximately 6×10^{10} cloud condensation nuclei (CCN) are produced for each gram of wood consumed in a fire. Eagan *et al.*, measured concentrations of CCN to 5000 cm^{-3} about 38 km downwind from a 4 ha prescribed fire. Most of the CCN are in the size range of approximately 0.10 μm (Reid and Hobbs, 1998). The presence of huge concentrations of CCN shifts fog droplet size distributions towards the lower end of the droplet size spectrum and increases the extinction coefficient.

Land managers in the southern United States (shaded area in Figure 1) use prescribed fire to treat 6–8 million acres (2–3 million ha) of forest and agricultural lands each year (Wade *et al.*, 2000). Although the vast majority of prescribed burns are carried out without incident, there are occasions when weather conditions combine with residual smoke to compromise visibility. Multiple-vehicle pileups, numerous physical injuries, extensive property damage, and fatalities have been associated with visibility reductions due to smoke or smoke and fog on roadways (Mobley, 1989). Most serious accidents occur during the night or near sunrise when smoke trapped within local drainage flows in stream valleys and basins (where ambient relative humidity may locally approach 100%) drifts across roadways.

* Correspondence to: Gary L. Achtemeier, USDA Forest Service, Southern Research Station, Center for Forest Disturbance Science, Athens, GA 30602, USA. E-mail: gachtemeier@fs.fed.us

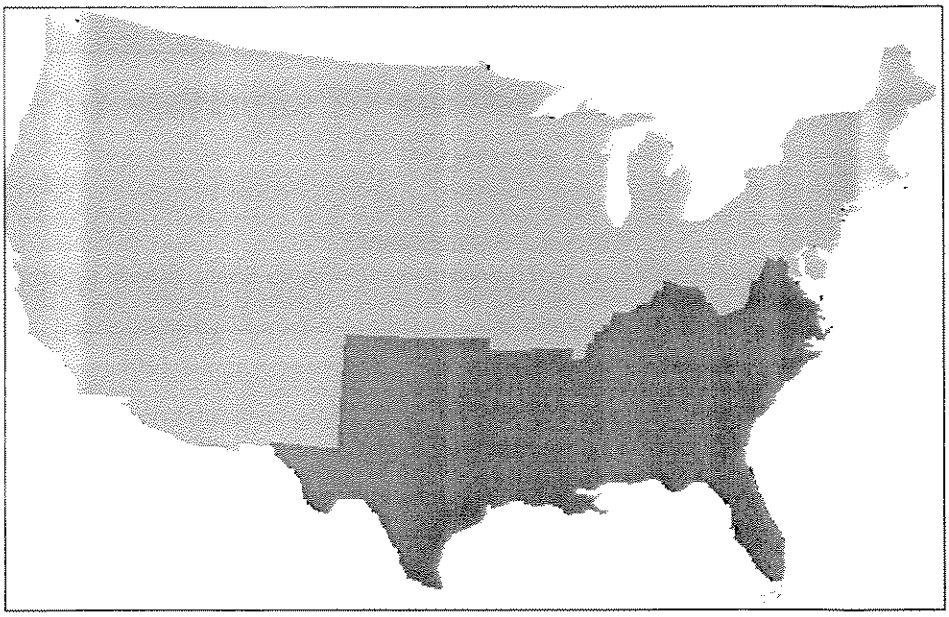

Figure 1. Map of the United States showing the region of extensive prescribed fire use during the winter/spring season.

Most prescribed burns are conducted during periods of high dispersion during the dormant season (January to April) after leaf/needle fall and before the emergence of new vegetation in the spring. This burn period coincides with the winter wet season and much burning is done when dry surface fuels overlay wet fuels so that not all of the available fuel will be consumed. Therefore, smoke could contain moisture released as part of the chemistry of combustion, moisture boiled off from wet fuels that subsequently ignite, and moisture released from heated soil and underlying fuels that do not ignite.

An analysis of temperature and relative humidity measurements from 29 'smokes' (defined as a tiny plume of smoke less than 30 cm across rising above a patch of smouldering fuel) during 2002 and 2003 by Achtemeier (2006) showed that moisture excesses from smoke have no impact on ambient relative humidity during daytime high dispersion conditions. However, at night, during low dispersion conditions, bulk moisture impacts from residual smoke spread over large burned tracts of land can be large enough to increase the ambient relative humidity to 100%. Therefore, smoke moisture may be a contributing factor to the location, timing and augmentation of fog.

However, there remained the question of how much smoke moisture could additionally reduce visibility in fog. Visibilities at some accident sites have been estimated to range from 1 to 3 m. (In this paper fogs reducing visibilities to less than 3 m are defined as 'superfog.') In addition, descriptions of smoke/fogs by witnesses ('Couldn't see my hand in front of my face'; 'couldn't see the ground at my feet') match descriptions given by observers of the famous London fogs (UK Meteorological Office).

Achtemeier (2008) re-examined the smoke data as individual smokes with a two step radiation/mixing model to determine whether non-gradient mixing (Gerber, 1991) in the presence of huge concentrations of CCN could support superfog. At the times of observation, the smokes were not saturated. However, if it was assumed that the smokes persisted through the night when ambient relative humidities ranged from 51 to 88%, the study found smoke LWC in the range from 1.0 to 5.1 g m^{-3} – up to 17 times greater than LWC for natural fog. These smoke LWC were sufficient to support superfog for fog droplet size distributions reported in the literature in the range of from 1 to 3 μm. Therefore, non-gradient mixing provides a fog-forming mechanism in addition to heavily polluted conditions.

Smokes measured by Achtemeier (2006, 2008) were not saturated. On 22 March 2003 the measurements were made for forest litter under ambient conditions more favourable for fog formation. Direct measurements of superfog were obtained. The data collection is described in the next section. Results and discussion of the mechanics of superfog formation and persistence follow.

2. Materials and methods

The experiment was done at North High Shoals, GA, on 22 March 2003. Leaf litter, consisting of a mixture of leaves fallen from hardwoods (mostly oak) and needles blown in from a nearby stand of loblolly pine (*Pinus taeda L.*) were raked into a shallow pile roughly 3 m in diameter. The moisture content of the leaves was not measured. However, with the presence of pine needles, there was concern that the leaves might not be sufficiently moist to retard rapid 're-flaming' of the pile – which did occur.

The pile was ignited at 1851 h local time (2351 UTC), 10 min after sunset. Winds were light and the protection offered by the surrounding woodland and a nearby

home further sheltered the burn. A temperature and relative humidity probe (Vaisala HMP45C, Vaisala, Inc.) mounted at the end of a 3 m pole was inserted into the smoke approximately 0.1 m above the litter pile to gain a continuous record of temperature and relative humidity. The operational temperature range was −40 to +60 °C. The response time for the relative humidity sensor was rated at 15 s. The response time for the temperature probe was estimated at from 3 to 5 min (slow-response) and difficulties with the use of this sensor for smoke measurements were described by Achtemeier (2006). Therefore, a 36-gauge type T Teflon-coated thermocouple (omega.com/temperature/Z/pdf/z223.pdf) was attached to the sensor. This instrument has an operational temperature range from −200 to +350 °C and an estimated sub-second response time (fast-response). Data from the Vaisala instrument and the thermocouple were recorded at 5 s intervals on a data recorder (CR23X Data Logger, Campbell Scientific, Inc.) attached to the opposite end of the pole supporting the instrument (Figure 2).

Once combustion was well established, the flames were smothered by raking unburned litter over the top of the flaming fuels. Re-flaming interrupted measurements at 3, 4, 12, and 15 min after the beginning of the measurements. Once the flames were smothered, dense white smoke was produced. The image in Figure 2 reveals a faint shadow of the probe extending into the plume. Given that none of the identifying marking was distinguishable, the visibility could have ranged from a few centimetres to approximately 0.1 m. A maximum visibility of 0.1 m has been assigned.

Figure 2 shows part of the fate of the superfog after it rose above the probe. The plume rose lazily to from 3 to 5 m above ground then levelled off and slowly settled to just above the ground. The period of time from superfog initiation to settling to the ground and the fate of the superfog thereafter were not observed as the measurements were being taken on the upwind side of the plume. Furthermore, attention was given to keeping the probe in the plume and watching for re-flaming. Finally, the experiment ended after dark.

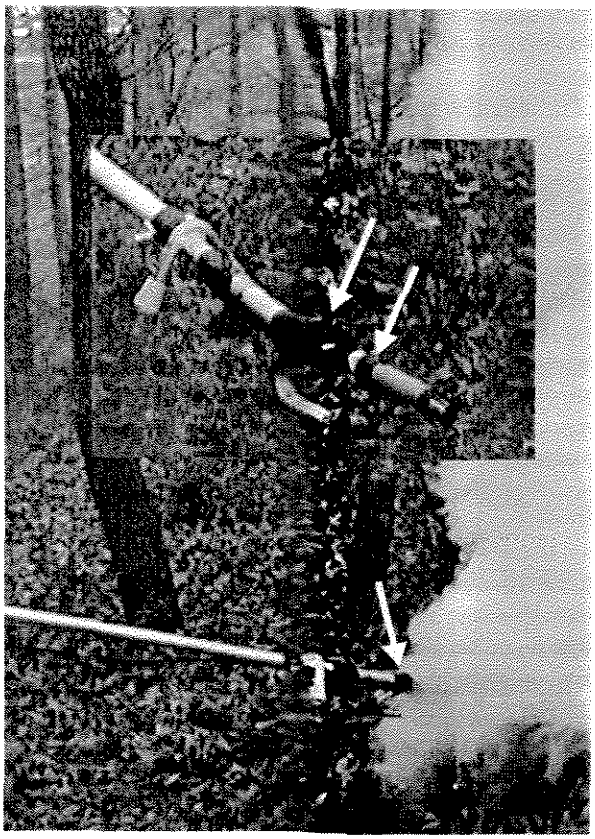

Figure 2. Upper inset – the Vaisala temperature and relative humidity probe attached to an extendable rod. The distance between the two arrows is 0.05 m. The distance from the attaching tape (arrow) to the tip of the probe is 0.12 m. Below – the probe inserted into a plume of superfog approximately 0.3 m wide. The arrow is the same as the upper left arrow in the inset. None of the remaining black strip, the white strip, the second black strip (second arrow), nor any of the probe are distinguishable in the image.

3. Results

Figure 3 shows the temperature and relative humidity records for the burn. The thin jagged line is the temperature trace for the fast-response thermocouple. The instrument was inserted into the smoke after flames were smothered – at 3, 4, 6–12, 14–17, and 22–26 min. Smoke temperatures were mostly in the range 40–60 °C with a few temperatures exceeding 70 °C between 6 and

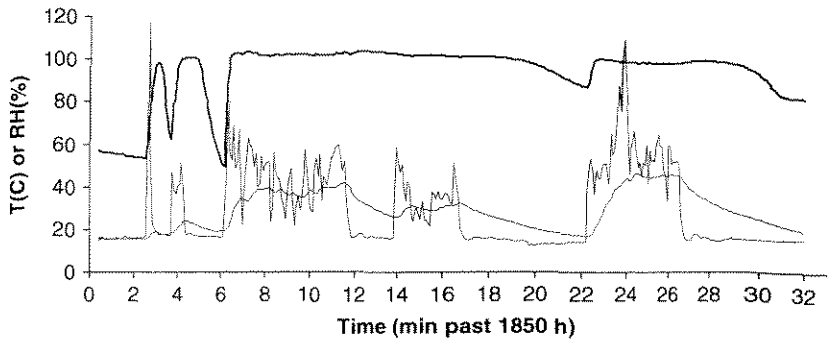

Figure 3. Fast-response temperature (thin jagged line), slow-response temperature (thin smooth line), and relative humidity (thick line) traces for the superfog experiment on 22 March 2003. Fast-response temperatures decreased to ambient temperature each time the instrument was withdrawn on flameup.

7 min and again between 24 and 26 min. Temperatures measured by slow-response sensor are shown by the thin smooth line.

The relative humidity plot (thick line) confirms that the white smoke was polluted fog. The ambient relative humidity was 58%. Each time the instrument was inserted into the smoke, the relative humidity jumped to 100%. Achtemeier (2006) showed that the temperature/relative humidity probe overestimated relative humidity when inserted into a warm smoke plume because of the connection between the moisture sensor and the slow-response temperature sensor. However, the slow-response temperature reached values measured by the fast-response thermocouple from 8 to 12 min and again from 24 to 26 min with no observed decline in the relative humidity.

Furthermore, Achtemeier (2006) showed that the sensor should have underestimated relative humidity when the instrument was withdrawn from a warm smoke plume. However, the relative humidity did not drop below the ambient relative humidity when the instrument was withdrawn but remained at saturation during 12–14 min between sample period 3 and 4. The behaviour of the relative humidity when the instrument was withdrawn from the plume for longer periods of time: (17–22 min and 27–32 min) was that of relative humidity slowly declining from 100% after having been removed from the smoke for at least 2 min. This behaviour would be expected if the instrument was wet and hot and water was slowly evaporating from the sensor.

The calculations of mixing ratio (defined as the mass of water vapour present to the mass of dry air containing the vapour – Hess, 1959) from temperature and relative humidity were done recognizing the following uncertainties. First, mixing ratios calculated using temperature data from the slow-response sensor were likely to be erroneously low because, with few exceptions, the temperature readings were too cool. Second, if the mixing ratios were calculated using temperatures measured with the high-response thermocouple, there was no certainty that relative humidities would have been 100% at these temperatures. However, that the fast-response temperature was the correct temperature within the plume is a reasonable assumption. Furthermore, given the presence of the dense white cloud during the measurements, and given the behaviour of the relative humidity sensor described above, it is reasonable to suppose that the cloud was saturated at the fast-response temperatures.

Therefore, Figure 4 gives calculated mixing ratios with both the slow- and fast-response temperatures. Slow-response mixing ratios may be fairly accurate estimates of actual moisture from 8 to 12 min and 24–26 min when slow-response temperatures were roughly equivalent to fast-response temperatures (Figure 3). Mixing ratios ranged from 40 to 50 g kg^{-1} and 55–60 g kg^{-1} respectively. Fast-response mixing ratios ranged from 40 to 80 g kg^{-1} and 60–80 g kg^{-1} respectively for the same periods with spikes as high as 200 g kg^{-1}.

Smoke released in smouldering fuels mixes with ambient air. Let m_1, T_1, and w_1 represent the mass (g), absolute temperature (K), and mixing ratio of water (g kg^{-1}) of the smoke, respectively, and let m_a, T_a, and w_a represent the mass, absolute temperature, and mixing ratio of water of the ambient air, respectively. The final state, upon mixing at constant pressure, is given by the weighted means,

$$T = \frac{m_1 T_1 + m_a T_a}{m_1 + m_a}$$
$$w = \frac{m_1 w_1 + m_a w_a}{m_1 + m_a} \quad (1)$$

The saturation mixing ratio for the mixed air, w_s, defined as the mass of water contained in a mass of humid air for which the relative humidity is 100%, cannot be represented by the weighted mean of the saturation mixing ratios for the smoke and ambient air. The saturation mixing ratio for the mixture is calculated from the Clausius-Clapeyron equation (Petterssen, 1956).

Data points representing the range of minimum and maximum slow-response temperatures and mixing ratios for the observation periods from 8 to 12 min and from 24 to 26 min were selected for the mixing part of this study. Other data points giving the range of fast-response temperatures and mixing ratios were selected as representative of the same observation periods. High and low spikes were omitted. These points are summarized in Table I along with the ambient temperature and mixing ratio.

Table II lists the outcomes when equal masses of smoke and ambient air are mixed. For the slow-response

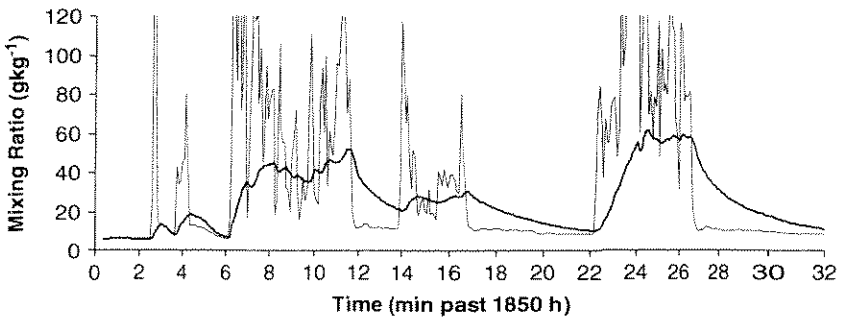

Figure 4. Mixing ratios calculated from the Vaisala HMP45C temperature and relative humidity probe – slow-response sensor (thick line) and from the relative humidity probe and temperatures measured by the fast-response thermocouple (thin line).

Table I. Ranges of slow- and fast-response temperatures and mixing ratios selected for mixing with ambient air.

Period min	Slow-response		Fast-response	
	Temperature °C	Mixing ratio g kg^{-1}	Temperature °C	Mixing ratio g kg^{-1}
8–12	34.8	34.69	40.3	46.70
	42.1	51.98	54.1	93.90
24–26	41.2	47.20	45.8	60.10
	46.4	61.65	62.5	134.34
Ambient	15.0	6.20		

Table II. Ranges of slow- and fast-response final temperatures, mixing ratios, saturation mixing ratios, and excess liquid water after mixing with equal masses of ambient air.

Period min	Slow-response				Fast-response			
	Temperature °C	Mixing ratio g kg^{-1}	Saturation M. ratio g kg^{-1}	LWC g m^{-3}	Temperature °C	Mixing ratio g kg^{-1}	Saturation M. ratio g kg^{-1}	LWC g m^{-3}
8–12	24.9	20.45	19.21	1.24	27.7	26.45	22.59	3.86
	28.6	29.09	23.81	5.28	34.6	50.05	33.45	16.60
24–26	28.1	26.70	23.19	3.51	30.4	33.15	26.48	6.67
	30.7	33.93	26.94	6.99	38.8	70.27	42.08	28.19

observation periods, mixing produced the ranges of temperatures and mixing ratios shown in the first two columns. Saturation mixing ratios were calculated from the Clausius-Clapeyron equation. Differences between the mixing ratios and the saturation mixing ratios are given as excess liquid water content (LWC). The ranges of, respectively, 1.24–5.25 and 3.51–6.99 g m^{-3} are water available to be converted into fog. The right side of Table II lists the results for the fast-response temperatures. The ranges of excess LWC are, respectively, 3.86–16.60 and 6.67–28.19 g m^{-3} are water available to be converted into fog.

4. Theoretical analysis and discussion

Liquid water contents for natural fog typically range between 0.001 and 0.30 g m^{-3} (May, 1961; Roach, 1976; Hudson, 1980; Meyer *et al.*, 1980; Kunkel, 1984; Cotton and Athens, 1989; Duynkerke, 1991; Fuzzi *et al.*, 1992; Teixeira, 1999; and Guedalia and Bergot, 1994). Achtemeier (2008) modelled LWC from the smoke temperature and moisture measurements in the range from 0.07 to 5.1 g m^{-3} – up to 17 times larger than LWC found in fogs forming under natural conditions. Depending on the temperature sensor used, the range of LWC found in this study is from 1.24 to 28.19 g m^{-3} – almost 100 times larger than LWC found in natural fogs.

The relationship between visibility and fog density is (Kunkel, 1984):

$$VIS = -\frac{\ln(\eta)}{\beta} \tag{2}$$

where β is the extinction coefficient given by,

$$\beta = \pi \sum_{i=1}^{N} Q_e n_i r_i . \tag{3}$$

Here η is the threshold of contrast (normally equal to 0.02), Q_e is the normalized extinction cross section, and n_i is the number density for droplets of radius r_i. If the droplet size distribution is not known, then an empirical formula must be used to relate LWC to β. Kunkel calculated extinction coefficients that ranged from 0.15 to 80.0 km^{-1} using data on natural fogs. Because the visibility was observed during the present study, the extinction coefficient can be calculated directly from Equation (2). On substituting 0.10 m for the visibility, the extinction coefficient is 39 120 km^{-1}, far outside the range of extinction coefficients reported in the literature (Eldridge, 1971; Pinnick *et al.*, 1978; Kunkel, 1984).

Additional factors that impact visibility are the age and history of fog. Many of the fogs reported in the literature had been active for hours giving time for microphysical processes to grow the droplets and create broad drop size distributions. For example, Fuzzi *et al.* (1992) found a bimodal droplet size distribution with the dominant

volume mode around 20 μm and a much smaller mode at 5–10 μm. Garcia-Garcia *et al.* (2002) found droplet size distribution peaks at 4, 10, and 20 μm with the dominant peak at 4 μm. Kunkel found mean diameters ranging from 7 to 10 μm. Matveev (1965) published dominant peaks in the range of 5–7 μm with a spectrum ranging from 2 to 16 μm.

The age of the superfog in this study was less than 3 s at the location of measurement. Thus it should be expected that the droplet size distribution would be constrained to a narrow range and the dominant droplet size would be found at the small droplet end of the droplet distribution permissible by the sizes of the cloud condensation nuclei (CCN) released in smoke. Smoke particles have been measured using sophisticated instruments ranging from the Differential Mobility Particle Sizer (DMPS) to methods for sizing particles based on their aerodynamic properties (Ward, 2001). A very pronounced number concentration peak was found in the size range of approximately 0.10–0.13 μm (Reid and Hobbs, 1998).

Matveev (1965) equations permit calculations of extinction coefficients and LWC for droplet size distributions near the lower end of the drop size spectrum. The extinction coefficient is:

$$\beta = 2\pi n r_m^2 \tag{4}$$

where n is the number of droplets and r_m is the root-mean-square (rms) radius for the size of the droplets. The LWC is calculated from:

$$LWC = \frac{4}{3}\pi n r_m^3 \rho_w \tag{5}$$

where ρ_w is the density of water (g cm^{-3}). Combining Equation (4) with (5) and substituting visibility for extinction coefficient through Equation (2) yields:

$$LWC = \frac{-\ln(\eta) r_m}{1500 VIS} \tag{6}$$

when r_m is given in μm, VIS is given in km, and LWC is given in g m^{-3}.

Figure 5 shows LWC needed to maintain five levels of visibility in superfog. For droplet size of 0.1 μm, an LWC of only 2.61 g m^{-3} is required to maintain a visibility of 0.1 m. The required LWC doubles if the droplet size is increased to 0.2 μm. These LWC fall within the ranges of LWC calculated for both slow-response and fast-response temperatures and for both sampling periods (Table II). Figure 5 also shows that the LWC for all visibilities equal to or greater than 0.1 m and for all droplet sizes in the sub-micron range 0.1–1.0 μm fall within the range calculated for the 24–26 min period using the fast-response temperature.

An additional issue regarding the efficacy of these calculations in describing the superfog observed on 22 March 2003 is whether there existed a sufficient number of CCN available for superfog to form. Holle (1970) and Eagan *et al.* (1973) estimated that approximately

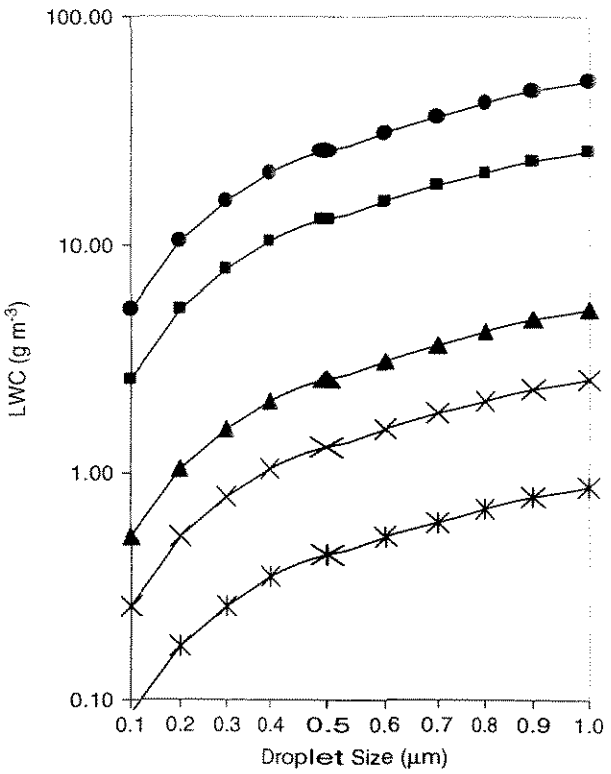

Figure 5. Liquid water content needed to maintain the following levels of visibility in superfog for the sub-micron range 0.1–1.0 μm: 0.05 m (circles), 0.1 m (squares), 0.5 m (triangles), 1.0 m (crosses), and 3.0 m (asterisks).

6×10^{10} cloud condensation nuclei are produced for each gram of wood consumed in a fire. Substitution of Equation (2) into (4) yields an expression for the number of CCN of radius r_m required to maintain an observed visibility:

$$n = \frac{-\ln(\eta)}{2\pi r_m^2 VIS} \tag{7}$$

The number of droplets of size of 0.1 μm required to maintain a visibility of 0.1 m is $n = 6.22 \times 10^8$ cm^{-3} – approximately 1% of the Holle (1970) and Eagan *et al.* (1973) estimate. If these particles make their way to the surface of the overlying vegetation without deposition at the rate of 0.01 m s^{-1}, then the rate of combustion for the smouldering forest litter would have been 0.01 g s^{-1} – for each square cm of burning litter – a not unreasonable rate of combustion given that the smouldering litter may have been several centimetres deep.

The results from theory have expanded on the observations to show the excess LWC and number of CCN required to produce superfog with visibility of 0.1 m. The LWC of 2.61 g m^{-3} is enormous when compared with the LWC of natural fog yet it is relatively small when compared with excess LWC calculated using fast-response temperatures (Table II). Conceivably, the large LWC could have been consumed in maintaining 0.1 m visibility as fog droplets grew rapidly from 0.1 to 1.0 μm (see the curve for $VIS = 0.1$ m (squares) in Figure 5). Alternatively, the LWC could have been expended through

mixing with ambient air as the superfog LWC was maintained near 2.61 g m^{-3}.

The fate of the excess LWC needs further explanation. The ranges of excess LWC in Table II were calculated from Equation (1) and the Clausius-Clapeyron equation and show the excess LWC that could have been available for superfog. However, Achtemeier (2008) suggested that mixing of ambient air with smokes occurs through surface mixing of undiluted cores initially. Thus one-to-one mixing may not accurately model the mixing between ambient air and the superfog on 22 March 2003. Furthermore, mixing *via* Equation (1) ignored the impact of latent heat release on the temperature of the mixed air mass.

Therefore the calculations for excess LWC were redone using a recursive model with the following steps.

1. Specified volumes of smoke and ambient air with the range of temperatures and moistures given in Table I were mixed *via* Equation (1) to give an initial estimate of the temperature and mixing ratio for the mixture.
2. The saturation mixing ratio was calculated from the temperature of the mixture via the Clausius-Clapeyron equation and subtracted from the mixture mixing ratio to yield the excess LWC.
3. Small increments of excess LWC were converted to liquid water with the resulting release of latent heat warming the mixed air mass slightly. The equation for air mass warming through latent heat release at constant pressure (Hess, 1959) is:

$$\Delta T = 2.49 \Delta w_s \qquad (8)$$

when the saturation mixing ratio is given in g m^{-3}.

4. Steps (2) and (3) were repeated until the temperature had increased until the mixture was just saturated.
5. The LWC required to complete step (4) was tallied as LWC available for conversion into fog.
6. Additional masses m_a were added to the existing mass of mixed air, m_i ($m_i = m_{i-1} + m_a$), and the procedure repeated until all available LWC had been released into fog.

At the end of Step (6) there resulted a mixed air mass, just saturated, with all excess LWC converted to liquid water, and with temperature, T_m, greater than the ambient temperature, T_a.

Any further mixing of the superfog with ambient air must involve evaporation of liquid water to bring unsaturated ambient air to saturation. The recursive model was continued with additional mixing; liquid water was removed from the fog and temperature was cooled through evaporation until no more liquid water remained (fog had dissipated) and the mixture was just saturated.

In doing the calculations with the recursive model, it was found that the results were dependent on the relative sizes of m_1 and m_a. If $m_a = m_1$ initially, the LWC tended to be approximately 15% higher after the first five mixes and the final LWC tended to be approximately 15% lower than if $m_a = 0.25\ m_1$ initially. Additional runs with other choices for the relative sizes of the constituents showed a tendency for the solutions to converge to near the $m_a = 0.25\ m_1$ solution. Thus the results to follow were done with $m_a = 0.25\ m_1$ initially.

Finally, the mixtures, mixture temperatures, and LWC were converted to rates of change of vertical velocity via:

$$W_t = \frac{m_i W_{t-1}}{m_i + m_a} + g\left(\frac{T_m - T_a}{T_a} - LWC\right)\Delta t \qquad (9)$$

The first term of Equation (9) reduces the vertical velocity in proportion to the mass of ambient air of $W_a = 0$ added to the existing mixture. The second term (Hess, 1959) adds the contribution to buoyancy by the temperature excess of the mixture decreased by the weight of liquid water *per* unit mass of air. Here Δt is a 'mixture time scale' set to $\Delta t = 0.075$ s to yield fog plume ascent heights comparable with the 3–5 m observed during the 22 March 2003 experiment.

The calculations were done for the fast-response (FR) temperatures and mixing ratios shown in Table I. An isothermal lapse rate with ambient temperature of 15 °C was used to facilitate the calculations and to show the impact of superfog on air mass temperatures. The calculations were stopped when (1) the fog LWC decreased to zero, or (2) the fog descended to spread out just above the ground. Figures 6 and 7 show the fast-response results for FR 8–12a (top row of Table I) and FR 24–26b (bottom row of Table I). These are representative of the range of fates of moist hot smoke injected into moist and cooler ambient air.

Contributions of temperature excess and weight of LWC to buoyancy are shown in Figure 6(a). The temperature excess term (dashed line) dominates the solution (solid line). The contribution of the weight of liquid water (dotted line) to the solution was insignificant. Calculations terminated at 2.5 s while the buoyancy was still positive. Vertical velocity (Figure 6(b)) increased to 0.3 m s^{-1} then levelled off after 1.7 s. Buoyancy was still positive but was balanced by addition of ambient air with zero vertical velocity into the mixture (first term of Equation (9)). Figure 6(c) shows the fate of the LWC as a function of height. LWC increased rapidly from 0 to 1.25 g m^{-3} in 0.4 s when the plume had risen to about 0.05 m above ground at 0.2 m s^{-1} (Figure 6(b)). Continued mixing with ambient air decreased plume LWC to zero in 2.5 s when the plume had risen to only 0.6 m above ground. Thus the calculations for FR 8–12a reveal a rising plume of smoke that flashed immediately into superfog which then thinned and dissipated a short distance above ground leaving a warm buoyant plume of smoke to rise and disperse.

Figure 7 shows the results for FR 24–26b. Temperature excess (dashed line) dominates the buoyancy term (Figure 7(a)) for the first 5 s. The temperature excess was then balanced by the weight of suspended liquid water (dotted line) as buoyancy dropped to zero by 7 s. Temperature excess fell below zero after 10 s meaning

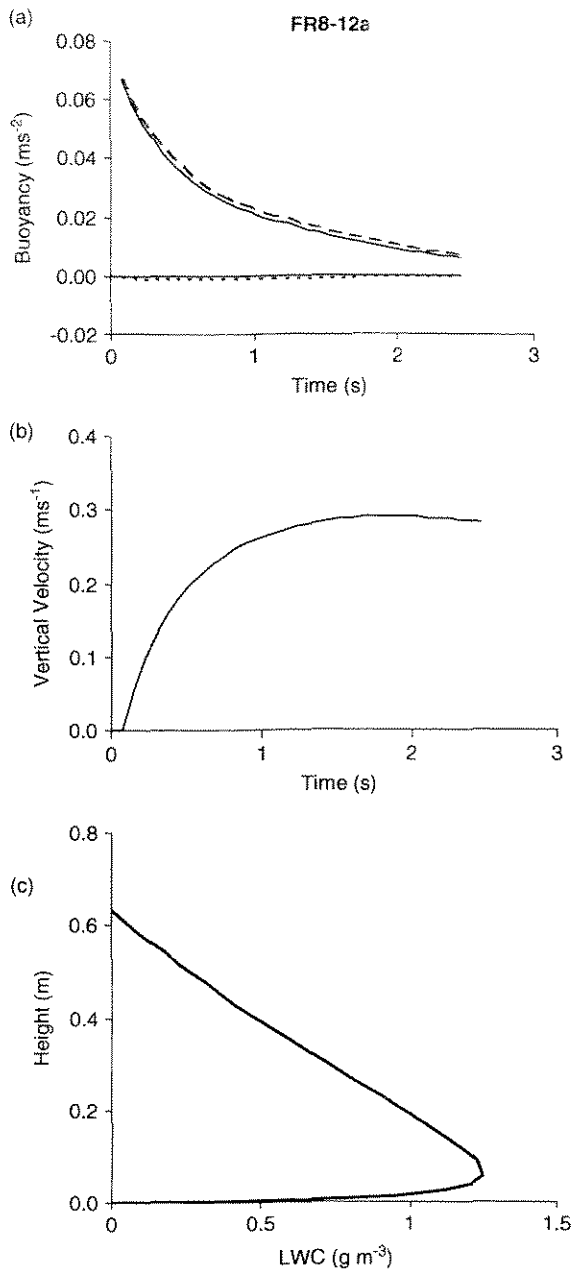

Figure 6. From Equation (9) for FR 8–12a: (a) Contributions to buoyancy (solid line) by temperature anomaly (dashed line) and weight of liquid water *per* unit mass of air (dotted line) for the 2.5 s duration of superfog. (b) Vertical velocity from buoyancy and non-gradient mixing. (c) Growth of LWC along the plume centre line from 0 to 1.25 g m^{-3} in the first 0.4 s of the solution followed by depletion through evaporation as the plume ascended to 0.6 m. This figure is available in colour online at www.interscience.wiley.com/ma

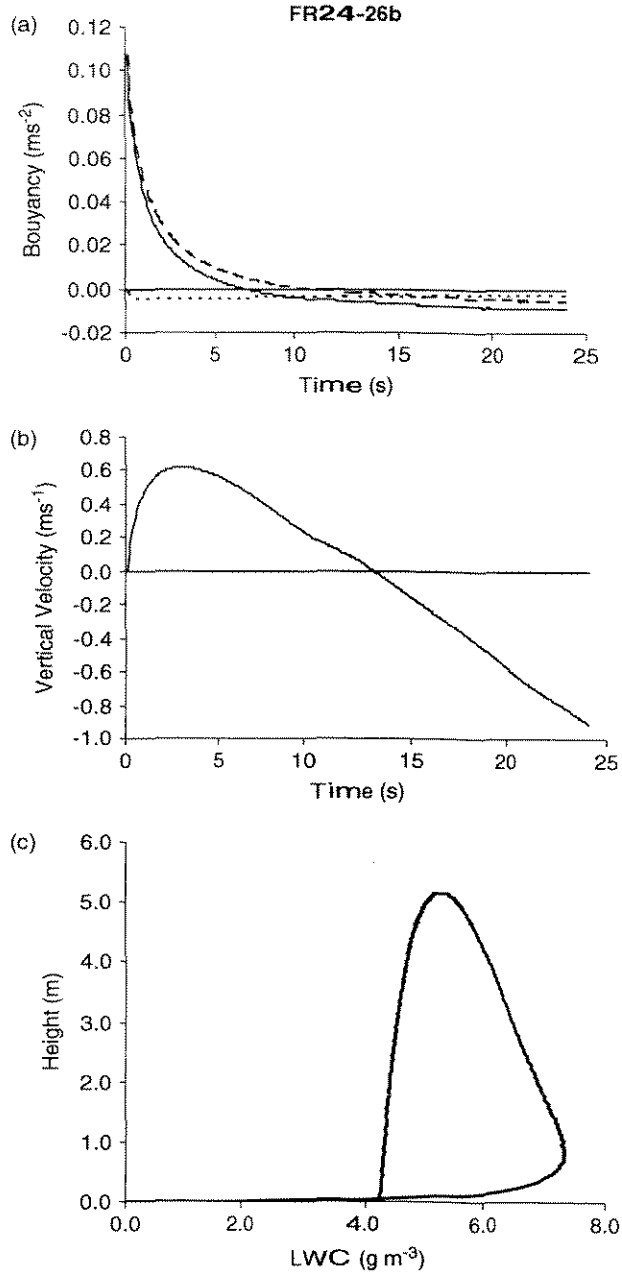

Figure 7. From Equation (9) for FR 24–26b: (a) Contributions to buoyancy (solid line) by temperature anomaly (dashed line) and weight of liquid water *per* unit mass of air (dotted line) for the 24 s duration of superfog. (b) Vertical velocity from buoyancy and non-gradient mixing showing sign reversal after 13 s. (c) Growth of LWC along the plume centre line from 0 to 7.34 g m^{-3} in the first 2 s as the plume ascended to 0.9 m. The plume ascended to 5.1 m while cooling through evaporation and then descended to spread out above the ground by 24 s.

the temperature of the mixture had cooled below the ambient temperature. Vertical velocity (Figure 7(b)) had increased to 0.6 m s^{-1} by 3 s then levelled off as the mixing term of Equation (9) balanced buoyancy. Vertical velocity decreased steadily thereafter to -0.8 m s^{-1} when the plume descended to spread out just above the ground after 24 s.

Figure 7(c) shows the behaviour of LWC during the 24-s period. LWC increased to 7.34 g m^{-3} during the 2 s that lapsed as the plume rose to 0.9 m above the ground at 0.59 m s^{-1} (Figure 7(b)). Thus, superfog continued to form and thicken as the plume drifted away from the emission source. LWC decreased through mixing and evaporation to 5.25 g m^{-3} as the plume ascended to its maximum height of 5.1 m above ground at 13 s (vertical velocity had decreased to zero). LWC then decreased to 4.25 g m^{-3} as the combination of negative buoyancy and weight of liquid water dragged the plume

down to spread out just above the ground after 24 s. Thus the calculations for FR 24–26b reveal a rising plume of smoke that flashed immediately into superfog capable of reducing visibility to the 0.1 m observed during the experiment. The plume remained superfog as the excess LWC declined through mixing and evaporation as the plume rose 5 m above ground. On further mixing, evaporation cooled the plume as it descended. Figure 5 shows that LWC of 4.25 g m^{-3} was capable of reducing visibility to less than 1.0 m for the full sub-micron range of fog droplet sizes.

The impact of the negative temperature anomaly (Figure 7(a)) needs further explanation. Cooling by evaporation of the superfog lowered mixture temperature below ambient temperature. Figure 8 shows that the superfog cooled to 12.7 °C creating a 'fog-generated' temperature inversion of 2.3 °C. This stable condition would inhibit further mixing.

The question remains as to what extent these results are transferable to superfog-producing smouldering in the aftermath of prescribed burning. Prescribed fire, particularly the many smaller burns, typically involves raking of litter similar to that in this study, to create fire breaks and to pile fuels as an aid to ignition. Smouldering occurs when oxygen-starved conditions slow rates of combustion to where gases cool to below ignition temperatures. Fire burning down into deep layers of fuel can be smothered by overlying burned fuel and ash. Furthermore, the energy required to evaporate water from surrounding moist fuels comes at the expense of combustion. Thus, given a wide range of possible fuel/moisture configurations in the field, there is no reason to suppose the methods used in this study produced uniquely different physical processes of smouldering.

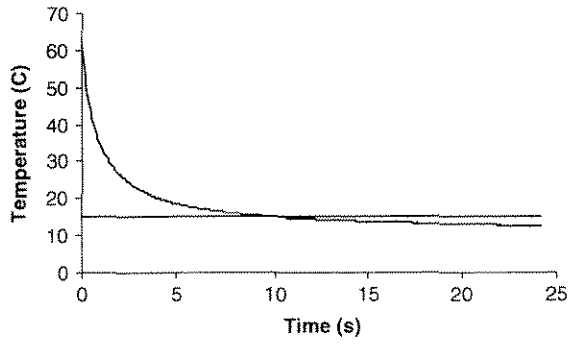

Figure 8. Temperature of the fast-response mixture FR 24–26b as the plume cooled *via* non-gradient mixing from 62.5 to 12.7 °C −2.3 °C below the ambient temperature of 15 °C (horizontal line). This figure is available in colour online at www.interscience.wiley.com/ma

What was the fate of the superfog after settling near the ground? The observations of 22 March 2003 provide no answer as efforts were focused on gaining the superfog measurements just above the litter. Furthermore, measurements were taken on the upwind side of the plume and thus downwind behaviour of the superfog was obscured by the plume. Finally, the experiment was completed after dark.

Extending the solutions from Equation (9) beyond those shown in Figure 7 is speculative because no provisions are made for fog droplet growth. However, Equation (9) can give qualitative estimates for the fate of the superfog. The solution for FR 24–26b was extended to 365 s when fog evaporated.

The first row of Table III lists the times elapsed from the start of the simulation. The second row shows LWC in decreasing order as the fog mixed away. Thus, the superfog settled to the ground after 24 s (Figure 7), LWC declined to 4.0 g m^{-3} after 28 s and 1.0 g m^{-3} after 178 s, and all fog dissipated by 365 s. The third row shows the maximum droplet size (μm) allowable to maintain minimal superfog of 3 m visibility. Had the LWC remained constant at 4.0 g m^{-3}, then fog droplets could have grown to 3.9 μm in superfog.

Equation (9) modelled additional plume characteristics. The fourth row of Table III shows the distance the plume would have travelled from its source assuming an average speed of 0.5 m s^{-1} – a reasonable wind for forest drainages during weather conditions that favour smoke entrapment (Achtemeier, 1993). If, after 178 s (when the LWC had declined to 1.0 g m^{-3}), the droplet size was less than 1.3 μm, a wind of 0.5 m s^{-1} would have carried superfog almost 90 m from its source. In addition, a unit plume volume would have grown almost 600 times from the mixing of ambient air into the plume. If the initial plume diameter was 0.3 m (Achtemeier, 2006), then the plume after 178 s (assuming a rectangular-shaped plume 3 m deep) would have been 14 m wide (bottom row of Table III). Thus, it is suggested that superfog from a single smoke could cause serious visibility hazards over roadways adjacent to the burn.

Finally, it can be supposed that visibility-obstructing superfog occurring 1–2 km downwind from a prescribed burn has as its source more than one superfog-producing smouldering smoke. Achtemeier (2006) showed that the net effect of many smokes spread over a landscape is to increase the moisture of the ambient air. However,

Table III. Growth characteristics required to maintain minimal superfog (visibility of 3 m) for a single plume as modelled from Equation (9).

Time elapsed (s)	28.0	51.0	93.0	178.0	250.0	338.0	365.0
LWC (g m^{-3})	4.0	3.0	2.0	1.0	0.5	0.1	0.00
Droplet size (μm)	3.9	3.0	2.2	1.3	0.6	0.1	–
Distance travelled (m)	14.0	25.0	46.0	89.0	125.0	169.0	182.0
Volume growth ratio	93.0	170.0	312.0	595.0	844.0	1135.0	1220.0
Plume width (m)	2.0	4.0	7.0	14.0	20.0	27.0	28.0

not all smouldering smokes produce temperature and moisture in the range required for the initiation of superfog (Achtemeier, 2008). This may explain partly why superfog events are relatively rare given the large number of prescribed burns carried out annually within the southeastern United States.

5. Conclusions

Non-gradient mixing of warm, moist smoke with cool, moist ambient air can release LWC in amounts sufficient to aid the formation of superfog. This moisture, in the presence of an enormous number of CCN particles released during combustion, can flash into fog droplets at the small end of the droplet size spectrum. The smaller droplets, in comparison with larger droplets, are more efficient scatterers of light and thus are more efficient reducers of visibility. Thus the combination of both particulate matter and moisture provides the mechanism for superfog formation from smoke released during smouldering combustion in the aftermath of prescribed burns.

The fate of superfog is critically dependent on moisture in both the smoke and the ambient atmosphere. When smoke mixes with ambient air, a range of outcomes are possible. (1) The mixture may be unsaturated and the smoke disperses. (2) The mixture may be saturated with excess LWC large enough to support superfog initially. Continued mixing quickly dissipates the superfog and the smoke disperses. (3) The mixture may be saturated with excess LWC large enough to support superfog initially. Additional mixing evaporates the liquid water but not before the mixture temperature has been cooled to below the temperature for ambient air. The plume descends to some equilibrium height as fog evaporates leaving a shallow layer of smoke entrapped above the ground. (4) The mixture may be saturated with excess LWC large enough to support superfog initially. Additional mixing evaporates some of the liquid water of the superfog and cools the mixture temperature to below the temperature for ambient air. The mixture sinks to spread out just above the ground as either fog or superfog depending on the residual LWC. The increased stabilization traps the superfog just above the ground and inhibits further mixing. Thus, superfog can persist indefinitely until dissipated by strong solar insolation or by turbulent mixing in strong winds.

These scenarios may explain in part the formation and persistence of dense urban fogs such as the historic London fogs including the Great Smog of 1952. The urban situation is complicated by the presence of multiple elevated sources (chimneys) spread over large areas. Smoke temperature and moisture may not be as extreme as those observed on 22 March 2003 (for example, FR 24–26b). However, a lack of extreme emission temperature and moisture can be compensated by modification of stagnant air masses over time by multiple sources. Evaporation of superfog would steadily moisten and cool the ambient air mass into which subsequent plumes of superfog rise and mix. The outcome could have been a progression through the superfog scenarios described above. Eventually an elevated layer of dense fog formed a few tens to hundreds of metres above the ground. This layer eventually descended to just above the ground as fog or superfog depending on the available LWC.

Finally, superfog may not be all that uncommon. Non-gradient mixing creates a potential for superfog formation whenever warm, moist polluted effluents mix with relatively cool, moist ambient air. These conditions are met by effluents from coal-fired furnaces (especially in winter) through chimneys and stacks of houses and factories (such as those of old London), steam vented at industrial sites, power plant cooling towers, and the burning of piles of leaves.

Acknowledgements

Funding was provided through the National Fire Plan 01.SRS.A.5. Ken Forbus and Tim Giddens of the USDA Forest Service, Forestry Science Research Laboratory, Athens, GA, are acknowledged for their contributions to equipment management and field measurements.

References

Achtemeier GL. 1993. Measurements of drainage winds along a small ridge. *Proceedings of the 86th Annual Meeting of the Air & Waste Management Association*, Denver, CO, 93-FA-155.06.

Achtemeier GL. 2006. Measurements of moisture in smouldering smoke. *International Journal of Wildland Fire* **15**: 517–525.

Achtemeier GL. 2008. Effects of moisture released during forest burning on fog formation and implications for visibility. *Journal of Applied Meteorology and Climatology* **47**: 1287–1296.

Achtemeier GL, Jackson W, Hawkins B, Wade D, McMahon C. 1998. *The Smoke Dilemma: A Head-On Collision! Transactions of the Sixty-third North American Wildlife and Natural Resources Conference*. Wildlife Management Institute: Orlando, FL; 415–421.

Bell ML, Davis DL. 2001. Reassessment of the lethal London fog of 1952: Novel indicators of acute and chronic consequences of acute exposure to air pollution. *Environmental Health Perspectives* **109**(Suppl. 3): 389–394.

Cotton WR, Athens RA. 1989. *Storm and Cloud Dynamics*. Academic Press: San Diego, CA; 883.

Duynkerke PC. 1991. Radiation fog: A comparison of model simulations with detailed observations. *Monthly Weather Review* **119**: 324–341.

Eagan RC, Hobbs PV, Radke LF. 1973. Measurements of cloud condensation nuclei and cloud droplet size distributions in the vicinity of forest fires. *Journal of Applied Meteorology* **13**: 553–557.

Eldridge RG. 1971. The relationship between visibility and liquid water content in fog. *Journal of the Atmospheric Sciences* **28**: 1183–1186.

Fuzzi S, Facchini MC, Orsi G, Lind JA, Wobrock W, Kessel M, Maser R, Jaeschke W, Enderle KH, Arends BG, Berner A, Solly I, Kruisz C, Reischl G, Pahl S, Kaminski U, Winkler P, Ogren JA, Noone KJ, Hallberg A, Fierlinger-oberlinninger H, Puxbaum H, Marzorati A, Hansson HC, Wiedensohler A, Svenningsson IB, Martinsson BG, Schell D, Gorgii HW. 1992. The Po Valley fog experiment 1989: An overview. *Tellus* **44B**: 448–468.

Garcia-Garcia F, Virafuentes U, Montero-Martinez G. 2002. Fine-scale measurements of fog-droplet concentrations: a preliminary assessment. *Atmospheric Research* **64**: 179–189.

Gerber H. 1991. Supersaturation and droplet spectral evolution in fog. *Journal of the Atmospheric Sciences* **48**: 2569–2588.

Guedalia D, Bergot T. 1994. Numerical forecasting of radiation fog. Part II: A comparison of model simulation with several observed fog events. *Monthly Weather Review* **122**: 1231–1246.

Hess SL. 1959. *Introduction to Theoretical Meteorology*. Henry Holt & Co.: New York; 362.

Holle RL. 1970. Effects of cloud condensation nuclei due to fires and surface sources during South Florida droughts. *Journal of Applied Meteorology* **10**: 62–69.

Hudson JG. 1980. Relationship between fog condensation nuclei and fog microstructure. *Journal of the Atmospheric Sciences* **37**: 1854–1867.

Kokkola H, Romakkaniemi S, Laaksonen A. 2003. On the formation of radiation fogs under heavily polluted conditions. *Atmospheric Chemistry and Physics* **3**: 581, 589.

Kunkel BA. 1984. Parameterization of droplet terminal velocity and extinction coefficient in fog models. *Journal of Climate and Applied Meteorology* **23**: 34–41.

Matveev LT. 1965. Fundamentals of General Meteorology: Physics of the Atmosphere. Gidrometeorologicheskoe Izdatel'stvo, Leningrad. (Translated from Russian, Israel Program for Scientific Translations, Jerusalem, 1967), 695.

May KR. 1961. Fog-droplet sampling using a modified impacter technique. *Quarterly Journal of the Royal Meteorological Society* **87**: 535–548.

Meyer MB, Jiusto JE, Lala GG. 1980. Measurements of visual range and radiation-fog (haze) microphysics. *Journal of the Atmospheric Sciences* **37**: 622–629.

Mobley HE. 1989. Summary of smoke-related accidents in the South from prescribed fire (1979–1988). American Pulpwood Association Technical Release. 90-R, 11.

Pagowski M, Gultepe I, King P. 2004. Analysis and modelling of an extremely dense fog event in southern Ontario. *Journal of Applied Meteorology* **43**: 3–16.

Petterssen S. 1956. *Weather Analysis and Forecasting. Vol. 2: Weather and Weather Systems*. McGraw-Hill: New York; 266.

Pinnick RG, Hoihjelle DL, Fernandez G, Stenmark EB, Lindberg JD, Hoidale GB, Jennings SG. 1978. Vertical structure in atmospheric fog and haze and its effect on visible and infrared extinctions. *Journal of the Atmospheric Sciences* **35**: 2020–2032.

Reid JS, Hobbs PV. 1998. Physical and optical properties of young smoke from individual biomass fires in Brazil. *Journal of Geophysical Research* **103**: 32,013–32,030.

Roach WT. 1976. On the effect of radiative exchange on the growth by condensation of a cloud or fog droplet. *Quarterly Journal of the Royal Meteorological Society* **102**: 361–372.

Teixeira J. 1999. Simulation of fog with the ECMWF prognostic cloud scheme. *Quarterly Journal of the Royal Meteorological Society* **125**: 529–552.

UK Met Office. The great smog of 1952, 4, http://www.metoffice.gov.uk/education/secondary/students/smog.html. Accessed 2005.

Urbinato D. 1994. London's historic "pea-soupers". EPA Journal, Summer 1994, 2, http://www.epa.gov/history/topics/perspect/london.htm.

Wade DD, Brock BL, Brose PH, Grace JB, Hoch GA, Patterson WA III. 2000. Fire in eastern ecosystems. In *Wildland Fire in Ecosystems~: Effects of Fire on Flora*, Brown JK, Smith JK (eds). Gen. Tech. Rep. RMRS-42. USDA Forest Service, Rocky Mountain Research Station: Fort Collins, CO; 53–96.

Ward D. 2001. Combustion chemistry and smoke. In *Forest Fires, Behavior and Ecological Effects*, Johnson EA, Miyanishi K (eds). Academic Press: San Diego, CA; 66.